IEEE Open Journal of Ultrasonics, Ferroelectrics, and Frequency Control

Received 15 February 2022; revised 5 April 2022 and 24 May 2022; accepted 6 June 2022.
Date of publication 14 June 2022; date of current version 28 June 2022.

Digital Object Identifier 10.1109/OJUFFC.2022.3182926

Nonlinearity of Piezoelectric Micromachined Ultrasonic Transducer Using AlN Thin Film

ZHIFANG LUO[1,2,3,4] (Student Member, IEEE), JUNXIANG CAI[1,2,3,4] (Student Member, IEEE), SONGSONG ZHANG[5,6], YUANDONG GU[5,6], LIANG LOU[5,6], AND TAO WU[1,2,3,4] (Senior Member, IEEE)

[1]School of Information Science and Technology, ShanghaiTech University, Shanghai 201210, China
[2]Shanghai Institute of Microsystem and Information Technology, Chinese Academy of Sciences, Shanghai 200050, China
[3]School of Electronic, Electrical and Communication Engineering, University of Chinese Academy of Sciences, Shijingshan, Beijing 100049, China
[4]Shanghai Engineering Research Center of Energy Efficient and Custom AI IC, Shanghai 201210, China
[5]School of Microelectronics, Shanghai University, Shanghai 200444, China
[6]Shanghai Industrial μTechnology Research Institute, Shanghai 201800, China

CORRESPONDING AUTHORS: L. LOU (liang.lou@sitrigroup.com) and T. WU (wutao@shanghaitech.edu.cn)

This work was supported in part by the National Natural Science Foundation of China under Grant 61874073, in part by the Natural Science Foundation of Shanghai under Grant 19ZR1477000, and in part by the Lingang Laboratory under Grant LG-QS-202202-05.

ABSTRACT We present the nonlinearity of Aluminum Nitride (AlN)-based Piezoelectric Micromachined Ultrasonic Transducer (PMUT) utilizing Laser Doppler Vibrometer (LDV) technique. The PMUT working at resonant frequency excite the piezoelectric layer into strong nonlinear region. The nonlinear phenomena are observed, such as frequency shift and nonlinear out-of-plane displacement magnitude. A mathematic model of piezoelectric nonlinearity is employed for analyzing the nonlinear behavior, and the second order piezoelectric coefficient is obtained subsequently. Approximately 120 harmonics, which are generated by PMUT nonlinearity, are obtained experimentally under a single-tone AC signal of a relatively high-level voltage. In addition, the number of harmonics can be controlled meticulously. Three different applications are developed to utilize harmonic generations in acoustic-optical hybrid microsystem and Radio Frequency (RF) field. The observation and analysis of AlN piezoelectric nonlinearity could benefit a further understanding of PMUT based on AlN thin film. We believe the generated harmonics can be potentially used in a wide variety of applications in signal processing and modulation.

INDEX TERMS Piezoelectric nonlinearity, piezoelectric micromachined ultrasonic transducer (PMUT), aluminum nitride (AlN).

I. INTRODUCTION

Many nonlinear mechanisms exist in the materials, such as dielectric nonlinearity [1], [2], elastic (mechanical) nonlinearity [3], [4], and piezoelectric nonlinearity [5], [6]. Piezoelectric nonlinearity can be observed when applying a larger AC force (for the direct piezoelectricity) or higher amplitude of AC electric field (for the reverse piezoelectricity). It was found that a linear increase of piezoelectric coefficient as a function of the applied pressure [7]. Piezoelectric nonlinearity in some kinds of piezoelectric materials has been investigated before, such as piezoelectric ceramics, and GaAs [5], [8], [9]. In the last century, Aurelle *et al.* measured the piezoelectric nonlinearity on transducers based on hard Lead Zirconate Titanate (PZT), and observed the spectrum splitting over the fundamental Frequency [5]. However, the nonlinear phenomena were found when the input voltage is higher than 35 V. Recently, the piezoelectric nonlinearity has been observed on soft PZT operating at 2 V [9]. The nonlinear properties based on GaAs have also been investigated. However, the nonlinearity of GaAs-based transducers requires low temperature (lower than 10 K) and high vacuum environment [10].

The harmonic generation is a typical nonlinear phenomenon [11], [12]. In general, the piezoelectric nonlinearity appeared on the transducers results in signal distortion and energy loss. However, the harmonics have a wide variety of applications in RF communications, quantum communications, and spectroscopy [13]–[15]. Most of the strategies for

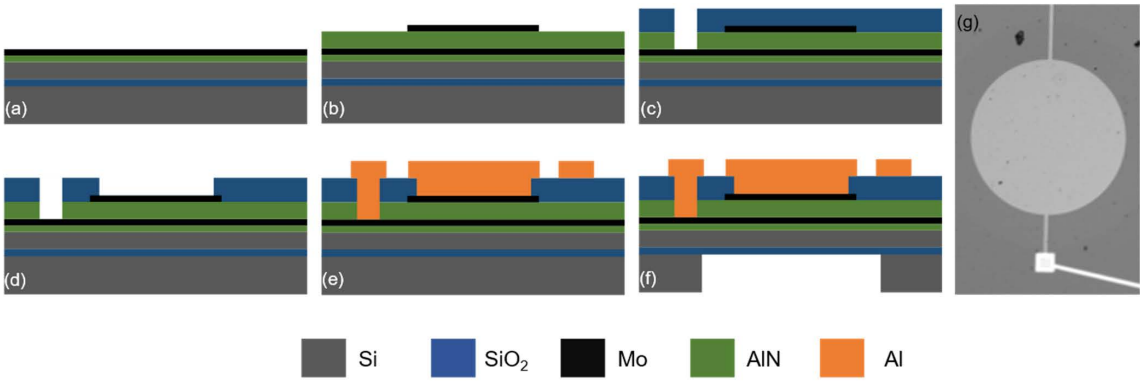

FIGURE 1. Fabrication process flow, (a) starting with SOI wafers with 5μm Si device layer, 20 nm AlN seed layer, and 200 nm Mo. (b) 1 μm AlN is sputtered, and 200 nm Mo is deposited and patterned. (c) 500 nm SiO_2 is deposited and etched as hard mask, then 1 μm AlN is etched and stopped on the Mo. (d) SiO_2 mask is etched. (e) 1 μm Al is deposited and patterned utilizing photoresist mask. (f) Grinding and DRIE the silicon at the backside. (g) Optical microscope image of PMUT with diameter of 500 μm.

harmonic generations need a complex experimental setup and high cost. At meanwhile, it is difficult to control the harmonic signals effectively.

The device with simple structure and high efficiency of harmonic generation is required for the promising future industrial applications. Due to the demand for low cost, small size, and high performance, Microelectromechanical Systems (MEMS) transducers may be the most promising technology for such requirement [16]–[18]. In recent years, piezoelectric MEMS has been a hot topic in electronic engineering, because of the high quality and great electromechanical coupling efficiency [19]–[21]. Aluminum Nitride (AlN)[22]–[26], Lithium Niobate (LN) [27], [28], and piezoelectric ceramics (PZT) [29] have been widely investigated in the past decades. So far, AlN thin film has been widely developed in piezoelectric transducers, due to its high phase velocity and CMOS compatibility [30]–[32]. Then, many researchers were curious about the interaction of acoustic wave with integrated optics based on these transducers, which could provide a useful approach to perform optical signal processing in a wide variety of applications[33]–[37]. The surface acoustic wave (SAW) [33], [38], [39], Lamb wave [34], and bulk acoustic wave (BAW)[37], [40] transducers have been widely studied in the acoustic-optical hybrid microsystems. However, most designs can only achieve Single-Input-Single-Output (SISO) acoustic-optic modulation [34]. To overcome the shortage of the existing technologies, the AlN-based PMUT is utilized. For the flexural vibrating, different vibrating modes generate unique patterns. Each higher-order harmonic signal corresponds to a particular mechanical vibration pattern. Then, the *n*-th higher-order harmonic vibration modes can modulate *n* different streams of photons. Thus, the concept of Single-Input-Multiple-Output (SIMO) can be achieved.

In this work, the PMUT based on AlN thin film is fabricated, then the electrical impedance and I-V characteristic are measured. Then, the first three resonant vibration modes are characterized, and the saturation of out-of-plane displacement is analyzed with observed piezoelectric nonlinearity of AlN PMUT. Next, the second order piezoelectric constitutive equations are provided to model the piezoelectric nonlinearity. In addition, the experimental harmonic generations are characterized, and then the promising applications are discussed. When the single-tone AC drive signal is applied to the PMUT, approximately 120 counts of modes are generated at the exciting voltage of 9 V_{pp}. The demonstrated nonlinear features and the disclosed potentialities of micro/nano device technology suggest that it is an excellent candidate for implementing compact, low-cost AlN-based transducers for SIMO communications.

II. FABRICATION

The PMUT was fabricated via a five-mask process, which starts with a SOI wafer. The SOI wafer is composed a 675-μm handling silicon, a 1-μm oxide, and a 5-μm device wafer silicon (100). Prior to the 1-μm AlN (0002) deposition, 20-nm AlN seed layer and 200-nm Mo (110) were sputtered (Fig. 1 (a)). After that, top 200-nm Mo layer was patterned as top electrode, and the loss of AlN layer was less than 50 nm (Fig. 1 (b)). Next, 500-nm low stress SiO_2 was deposited utilizing plasma enhanced chemical vapor deposition (PECVD) as etching hard mask; the bottom via and top via are etched utilizing reactive ion etch (RIE), as illustrated in Fig. 1 (c) and Fig. 1 (d). Then, 1-μm Al was deposited and patterned as pad electrode (Fig. 1 (e)). Lastly, a grinding process was utilized to reduce the bulk silicon thickness to 400 μm, and then the acoustic cavity of PMUT was defined at the backside by a deep reactive ion etch (DRIE) of the silicon; The theory and modeling of the acoustic cavity etched beneath the PMUT is investigated by the Shelton *et al.* [41]. The loss of oxide layer should be less than 50 nm (Fig. 1 (f)). The optical image of the fabricated PMUT is shown in Fig. 1 (g), the diameter of top electrode is 500 μm, which is the 70% of membrane diameter.

III. DEVICE CHARACTERIZATION

A. ELECTRICAL IMPEDANCE AND I-V MEASUREMENT

The electrical impedance of our PMUT was characterized by the impedance analyzer (Keysight E4990A). The sweeping

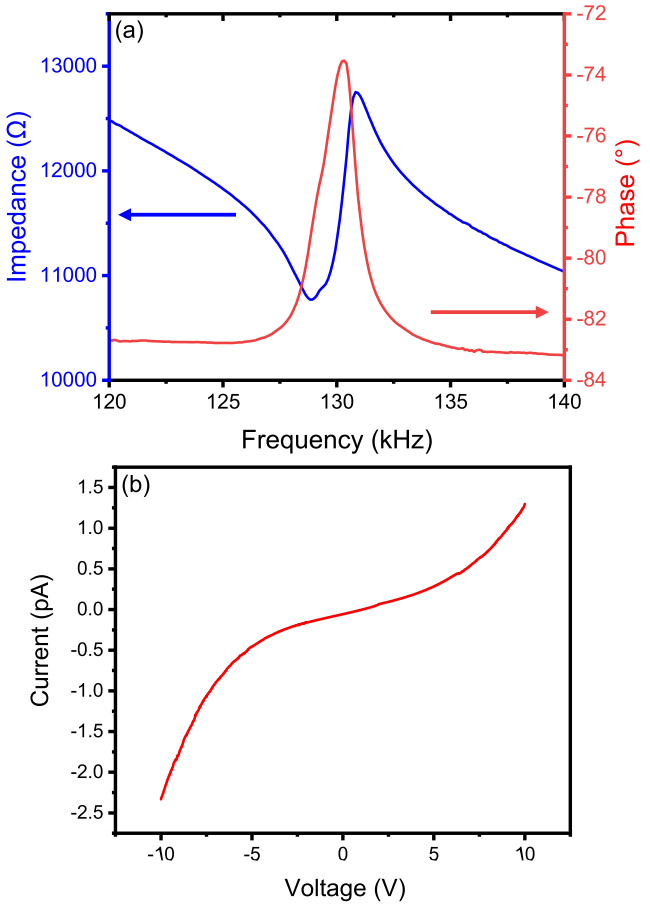

FIGURE 2. (a) The measured electrical impedance and phase of the PMUT. The frequency spans around the resonant frequency from 120 kHz to 140 kHz. (b) The measured I-V curve of PMUT.

frequency was set from 120 kHz to 140 kHz. Fig. 2 (a) shows the electrical impedance and phase of the PMUT. The resonant frequency of mode (0,1) of measured PMUT is about 127.5 kHz. The definition of mode (m, n) has been delivered by the Galerkin method[42], where the m and n are the numbers of resonant and anti-resonant peaks in the length and width directions, respectively. The electromechanical coupling coefficient k_t^2 was measured utilizing resonant and anti-resonant frequencies of PMUT. The k_t^2 can be expressed as,

$$k_t^2 = \frac{\pi^2}{8} \times \frac{(f_a^2 - f_r^2)}{f_a^2} \tag{1}$$

where the f_r is resonant frequency, while $f_a$is the anti- resonant frequency. The measured k_t^2 is 3.75%.

The Current-Voltage (I-V) measurement of the PMUT was conducted to identify the electrical standability of the AlN thin films under high electric field utilizing semiconductor device analyzer (Keysight B1500A), as shown in Fig. 2 (b). The current rised, when voltage increased from -10 V to 10 V. The asymmetry of the curve is due to the different configuration of top and bottom electrodes. None of the breakdown phenomenon have be discovered under 100 kV/cm.

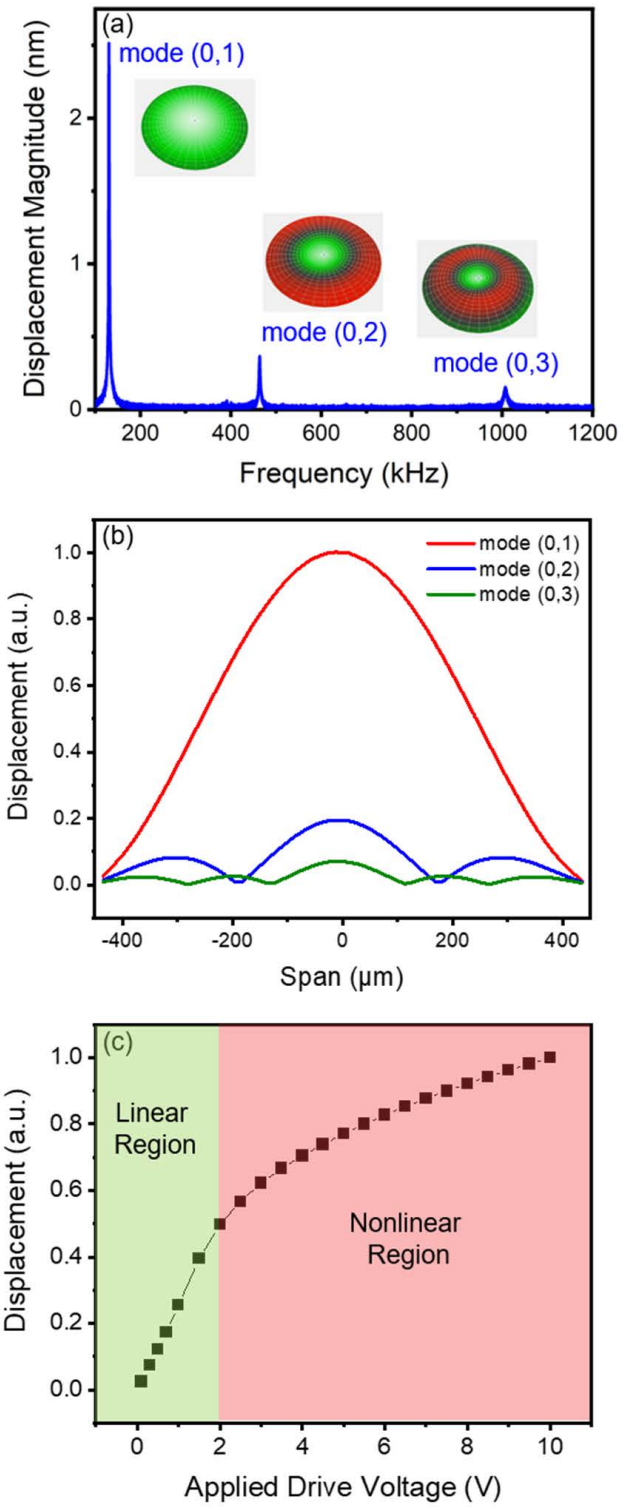

FIGURE 3. (a) Measured out-of-plane displacement magnitude and mode shapes of PMUT, the name of modes is determined by the Galerkin method. (b) The normalized displacement of mode (0,1), (0,2), (0,3), respectively. (c) The displacement magnitude of mode (0,1) under different input voltages.

B. OUT-OF-PLANE VIBRATION RESPONSE

The out-of-plane vibration response at the center of PMUT was observed by LDV (Polytec MSA-600 Micro System

Analyzer). As shown in Fig. 3 (a), the out-of-plane vibration displacement magnitude of the first three modes and the mode shapes are obtained, driven by 1 V_{pp} sweeping frequencies from 100 kHz to 1.2 MHz. The resonant vibration modes of mode (0,1), mode (0,2), and mode (0,3) were captured at 127.5 kHz, 458 kHz, and 995 kHz, respectively. The measured resonant frequency of mode (0,1) is consistent with the result from electrical impedance measurement. As shown in Fig. 3 (b), the normalized displacement of the first three modes along the axis of diameter was measured. Then, the out-of-plane vibration displacements of mode (0,1) under different applied voltages were also characterized utilizing LDV. The 127.5 kHz single tone AC signal was applied to excite the vibration of mode (0,1). As seen in Fig. 3 (c), when the applied voltage is under 2 V_{pp}, the PMUT works in the linear region, and the displacement magnitude has a linear relation with the amplitude of input signal. However, when the input voltage is over 2 V_{pp}, the PMUT goes into the nonlinear region. The saturation behavior of out-of-plane displacement with electrical drive signal can be explained in terms of the increase of viscous factor with larger input voltage. The signal tone AC signal has much higher voltage than the sweep signal, so the measured displacement magnitude shown in Fig. 3 (c) is much larger than that shown in Fig. 3 (a).

IV. PIEZOELECTRIC NONLINEARITY CHARACTERIZATION

To characterize the nonlinear piezoelectric response of AlN thin film, the displacement amplitude of AlN-based PMUT was measured. In our experiment, the PMUT was driven by AC signals of input frequency (f_{in}) from 100-150 kHz with different drive voltages, and the out-of-plane vibration response was captured by LDV. As shown in Fig. 4 (a), when the input voltage is below 3 V_{pp}, the PMUT is operating in the linear region. However, with a higher input voltage amplitude, the piezoelectric nonlinear behavior appears. The resonant frequency shifts towards the high frequency side, and the displacement magnitude shows the discontinuity. As the signal frequency is swept from low to high, the displacement response gradually increased to the maximum at resonant frequency, then dropped sharply. Then, the harmonics were measured near the center of the PMUT, when applying the single tone frequency f_{in}(equal to f_r) signal. If the input frequency f_{in} is close to the resonant frequency of PMUT mode (0,1), the resonance mode can be excited. Once the applied voltage with input frequency f_{in} is high enough, the higher order harmonics can be detected using LDV. The n^{th}harmonic has n times of resonant frequency f_0 of general vibrating modes with lower displacement magnitude, as shown in Fig. 4 (b).

V. MATHEMATIC OF PIEZOELECTRIC NONLINEARITY

In conventional situations, the AlN-based PMUT based is operated in a linear region. When a single AC signal is applied to the device, the device only operates at the given frequency. However, at a high-level drive, the piezoelectric thin film will

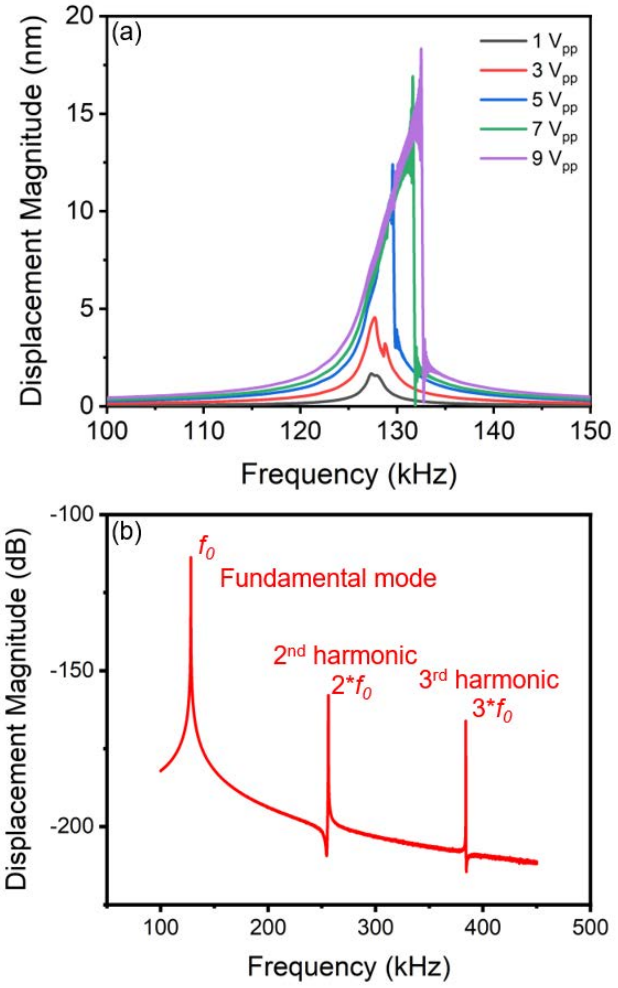

FIGURE 4. (a) Piezoelectric nonlinear behavior of PMUT by applying different drive amplitudes. (b) The generated harmonics by applying the single tone signal of 9 V_{pp} driving voltage.

be driven into a nonlinear region because of piezoelectric nonlinearity. The energy is speared over a discrete spectrum. A single-tone AC signal of f_{in}applied to the transducer can generate integral multiples of f_{in}.

To model nonlinear transducer behavior, we propose a second-order extension of the piezoelectric constitutive equations of AlN-based PMUT utilizing Taylor extension (the electrode thickness is neglected),

$$\begin{aligned} S(T,E) = S(0,0) &+ T\frac{\partial S}{\partial T}\Big|_{T=0,E=0} + E\frac{\partial S}{\partial E}\Big|_{T=0,E=0} \\ &+ T^2\frac{\partial^2 S}{2\partial T^2}\Big|_{T=0,E=0} + E^2\frac{\partial^2 S}{2\partial E^2}\Big|_{T=0,E=0} \\ &+ TE\frac{\partial^2 S}{\partial T\partial E}\Big|_{T=0,E=0} \end{aligned} \tag{2}$$

where S is the strain, T is the stress, E is the electric field. We assume that there is no pre-strain S_0 in PMUT ($S_0 = 0$).

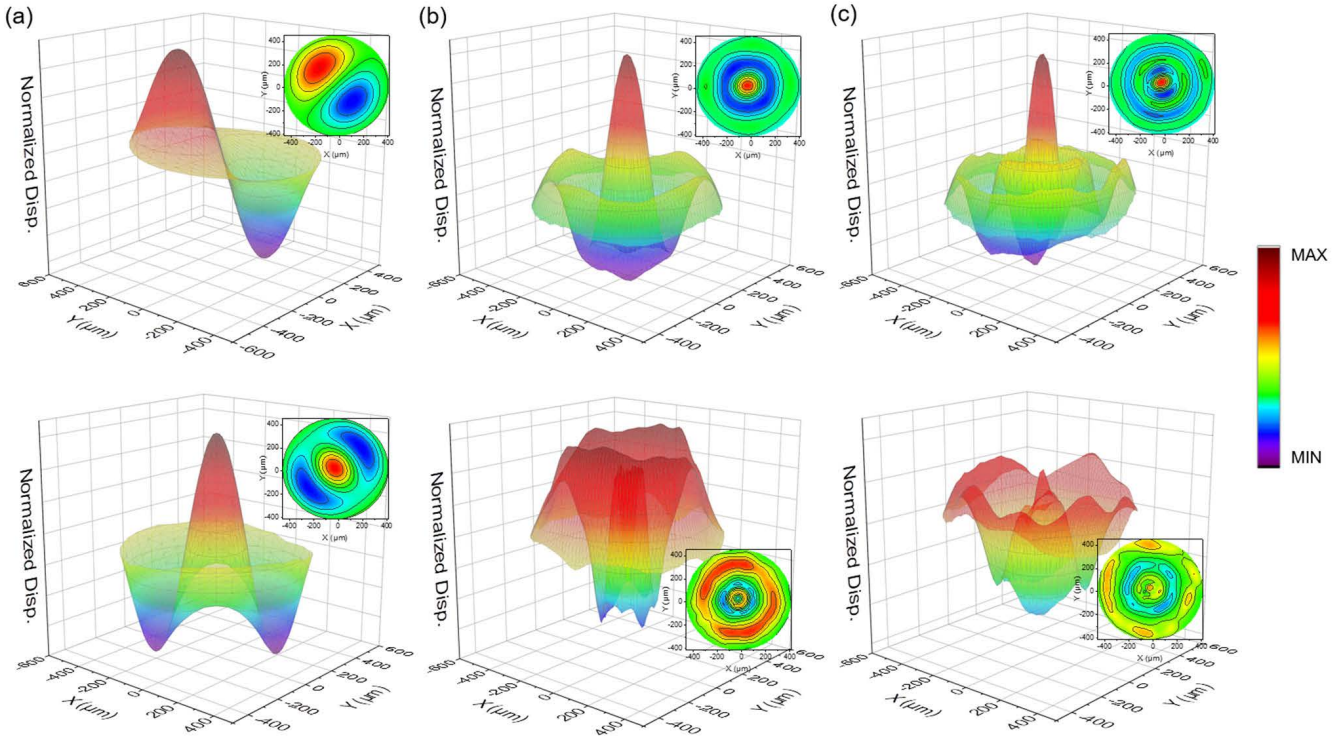

FIGURE 5. 3-Dimensional vibration map of (a) 2nd and 3rd harmonic mode-shapes of mode (0,1); (b) 2nd and 3rd harmonic mode-shapes of mode (0,2); (c) 2nd and 3rd harmonic mode-shapes of mode (0,3). The inserts are the 2-Dimensional contour map for each harmonic. The generated harmonics are formed by the piezoelectric nonlinearity of AlN.

Thus, Eq. (2) can be simplified and rewritten as,

$$S = cT + dE + \alpha T^2 + \beta E^2 + \gamma TE \tag{3}$$

where $c = \frac{\partial S}{\partial T}$ is the compliance, and $d = \frac{\partial S}{\partial E}$ is the piezoelectric charge coefficient. $\alpha = \frac{\partial^2 S}{2\partial T^2}$, $\beta = \frac{\partial^2 S}{2\partial E^2}$, $\gamma = \frac{\partial^2 S}{\partial T \partial E}$ are the nonlinear piezoelectric coefficients, respectively. Since the PMUT is mainly driven by electrical field, and no stress is provided to the PMUT ($T = 0$), Eq. (3) can be further simplified as,

$$S = dE + \beta E^2 \tag{4}$$

For the one-dimensional model of PMUT, the vibration direction of PMUT can be defined in the z-axis, and the strain in the x-axis can be expressed as,

$$S = \frac{\partial u}{\partial x} \tag{5}$$

Substituting Eq. (5) in Eq. (4), then we get,

$$\frac{\partial u}{\partial x} = dE + \beta E^2 \tag{6}$$

The approximation gives: $\frac{\partial u}{\partial x} = \frac{u}{R}$, where R is the radius of diaphragm. Thus, the Eq. (6) can be written as,

$$u = RdE + R\beta E^2 \tag{7}$$

The Eq. (7) can be treated by utilizing successive approximation, the displacement magnitude u can be divided into,

$$u = u_0 + u_1 + u_2 + \cdots + u_{n-1} + u_n \tag{8}$$

where the u_0 means the displacement magnitude of the linear vibration. u_i $(1 \leq i \leq n)$ are the displacement magnitudes of i^{th} harmonic vibration due to the nonlinear behavior. Then the Eq. (7) can be solved as,

$$\begin{cases} u_0 = RdE \\ u_1 = R\beta E^2 \end{cases}$$

It can be seen that $u_0$has the same frequency with E of f_0. While u_1 and E have same frequency f_1, which is the two times of f_0. If we extend the piezoelectric constitutive equations into n^{th}-order, u_i $(1 \leq i \leq n)$ would all be solved to have the frequencies of $i * bf_0$ in the frequency spectrum.

According to the equations above, the nonlinear piezoelectric coefficient β can be extracted utilizing the data in Fig. 4 (b). At applied voltage of 9 V_{pp}, the $\beta \approx 1.3 \times 10^{-18}$.

VI. APPLICATIONS

A. ACOUSTIC-OPTICAL MODULATOR

The demonstration of SIMO acoustic-optical modulator was performed utilizing Doppler effect by the monochromatic laser and the single frequency AC signal utilizing electric-in and mechanical-out arrangement. The laser head was directly set above the PMUT. In this experiment, the 7 V_{pp} AC signal was applied to the PMUT, such high-level driving voltage would excite the PMUT into the nonlinear region. As we have illustrated before, the frequency of drive signal needs to be set near the resonant frequency of the desired flexure mode. The reconstructed mode shapes of harmonics are shown in Fig. 5. The second and third harmonic mode shapes

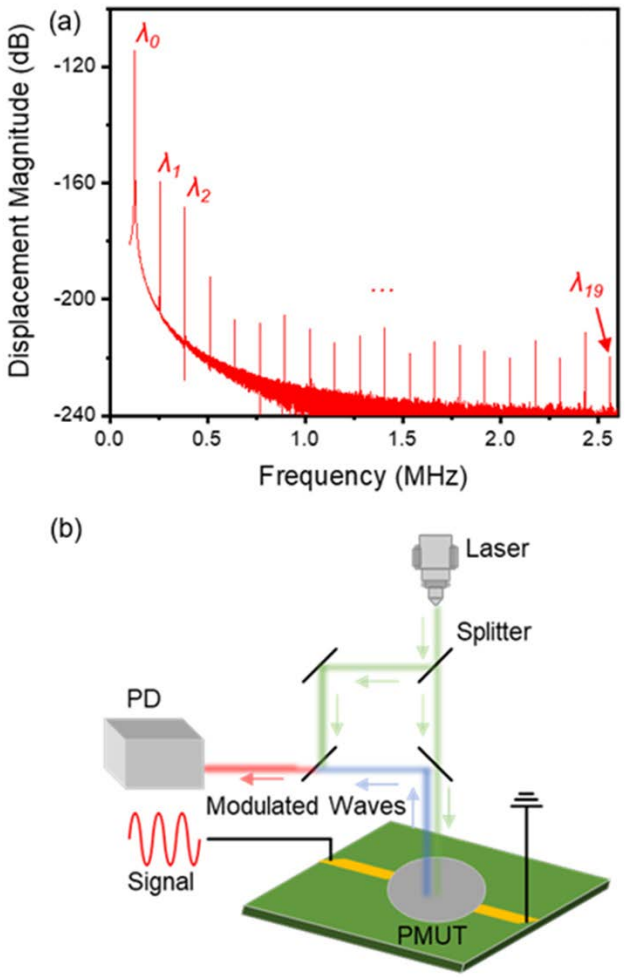

FIGURE 6. (a) The illustration of acoustic-optical modulation. (b) The diagram of the acoustic-optical modulation setup.

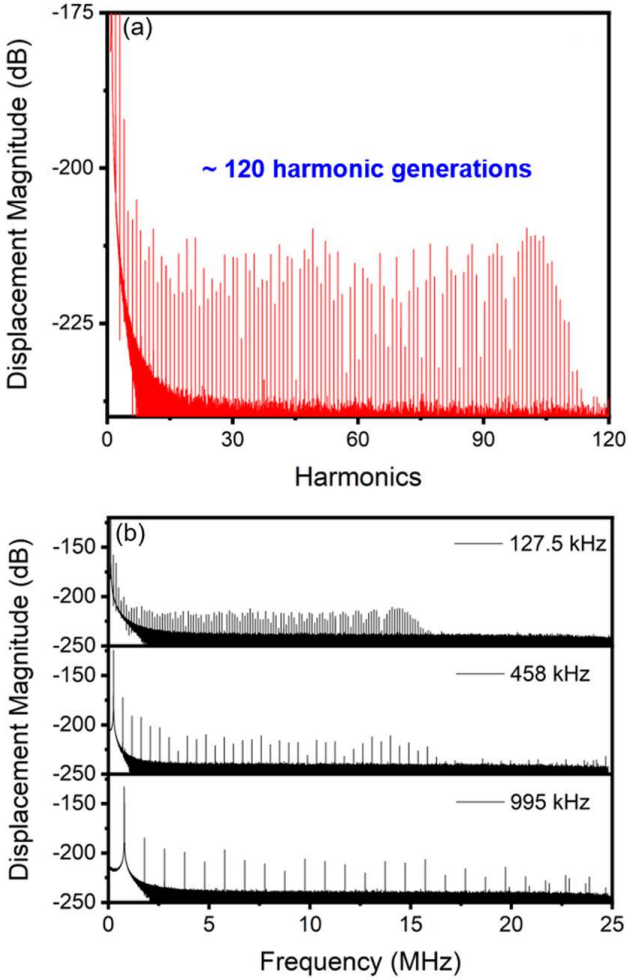

FIGURE 7. (a) The illustration of the number of generated harmonics at 7 V_{pp}; (b) The harmonic generations of PMUT based on first three resonance modes under the single tone AC frequency of driving voltage.

of modes (0,1), (0,2), and (0,3), respectively. It is clearly shown that these mode shapes are different in both pattern and magnitude. When the harmonic modes are excited at a time, the laser will be modulated by the multiple generated acoustic waves simultaneously. Due to the totally different patterns and working frequencies of 2nd to n^{th} generated harmonic mode shapes, when n harmonic modes are generated, the n-channels of optical waves with different frequencies and phases are modulated. As seen in Fig. 6 (a), optical signals with different wavelengths (λ) can be modulated in terms of the excited harmonics. In the frequency range of 0 to 2.6 MHz, up to 20 branches of optical signals are modulated utilizing acoustic-optical interactions. The schematic of modulation is shown in Fig. 6 (b). The original laser light splits into two beams for measurement and reference, respectively. After the input laser reaches the PMUT, the modulated optical will be reflected back. Finally, the modulated and reference waves both travel to the photodetector (PD).

Such multi-channel acoustic-optical modulation concept can also be utilized in the platform of AlN integrated optics in the future. The AlN-based waveguide can be directly integrated with PMUT. Due to the different stress generated in the piezoelectric layer by each harmonic, the refractive index of AlN will be influenced simultaneously by the stress-optical coefficient. Thus, the optical mode and phase of light can be modulated.

B. FREQUENCY COMB GENERATOR

In this section, the demonstration of frequency comb generator was provided by electrically driving the single PMUT into a highly nonlinear region. As shown in Fig. 7 (a), when the input voltage near the resonant frequency is 7 V_{pp}, the number of detectable harmonics by LDV spans from 0 to 25 MHz. The count of generated harmonics is approximately 120. Recently, Pillai [9] have demonstrated a SIMO frequency synthesizer utilizing a 2-port resonator based on PZT. With a driving power of 10 dBm, a train of harmonics is generated, and the harmonic counts are 108. In this experiment, the drive signal near the resonant frequency of mode (0,1) was applied, and the output vibration signal was detected by LDV. The output voltage signal has a positive relation with the detected displacement magnitude. As shown in Fig. 7 (b), the mode

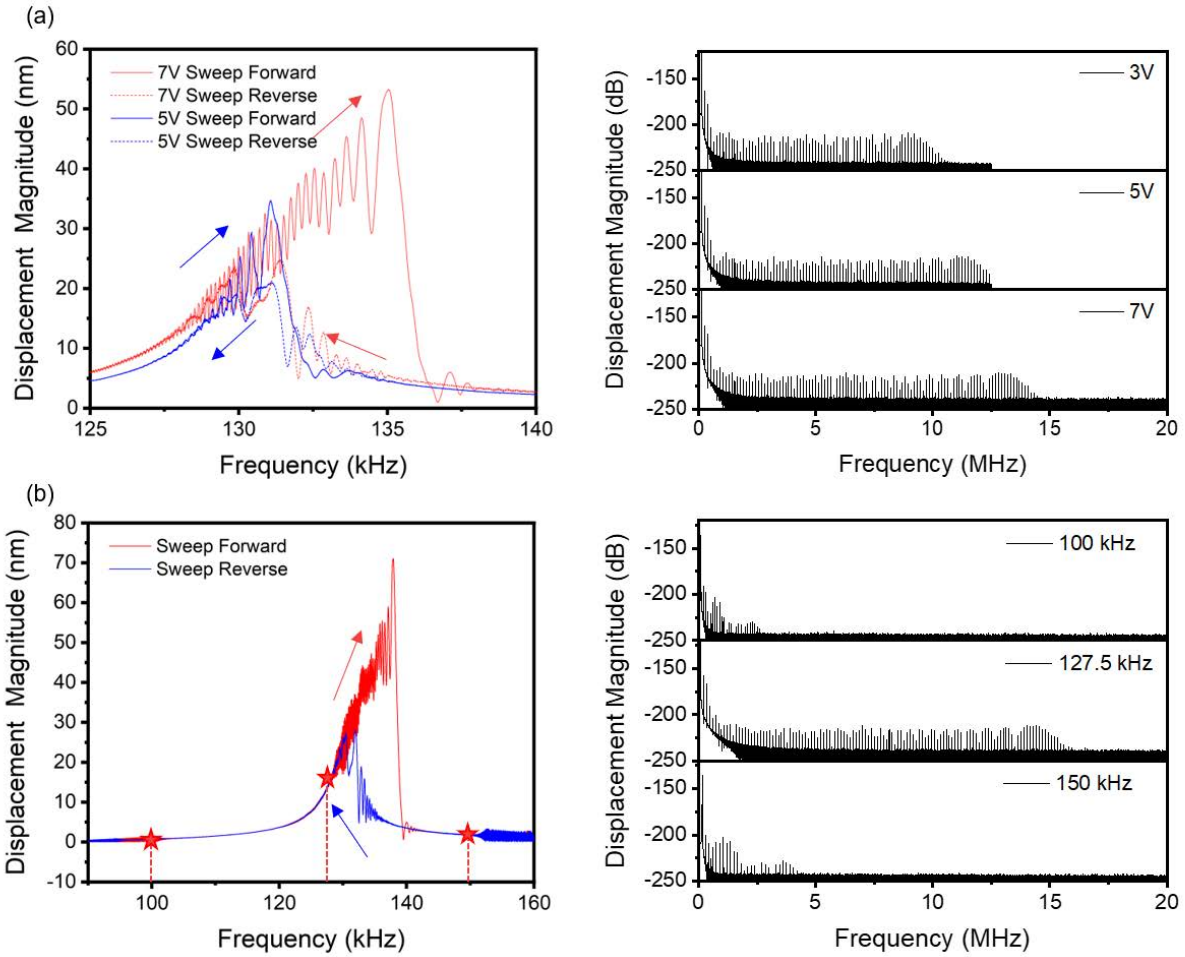

FIGURE 8. Illustrations of electrically controlled harmonic generations. (a) The plot of out-of-plane displacement magnitude for forward and reverse sweep of the PMUT from 125 kHz to 140 kHz corresponding to 5 V_{pp} and 7 V_{pp} are provided, and the displacement magnitude with three different input voltages are presented. (b) The plot of out-of-plane displacement magnitude for forward and reverse sweep of the PMUT from 90 kHz to 160 kHz is provided, displacement magnitude under three different frequencies are measured. The red dashed line and symbols are the guide for the eye.

(0,2) and mode (0,3) of PMUT could also successfully excite the frequency comb when the 458 kHz and 995 kHz single tone AC signals are applied to the PMUT, respectively. The output frequency combs are equally spaced in terms of the resonant frequency. Because of the higher resonant frequency of higher resonant mode than that of mode (0,1), a larger frequency range of frequency comb can be achieved, and more optical waves can be modulated in a wide frequency range.

Our observations can be utilized in RF communications in the future. The multi-channel oscillators can be implemented by working in the *n* different frequencies.

C. ELECTRICALLY CONTROLLED HARMONIC GENERATION

If the number of harmonic generations can be fully electrically controlled, the piezoelectric nonlinearity of AlN-based PMUT could be widely used. In this section, two different approaches, applying driving voltages in the nonlinear region and tuning the frequency of the given signal, were provided to achieve electrically controlling of the harmonic generations. In our observation, the harmonic generations are determined by the displacement magnitude. Larger out-of-plane displacement results in more harmonic generations. Moreover, when sweeping the cyclic frequency, the displacement magnitude appears hysteresis response.

The left panel of Fig. 8 (a) shows the nonlinear behavior for the forward and reverse frequency sweep of PMUT. The sweeping frequency is set from 125 kHz to 140 kHz to cover the resonant frequency of PMUT. For the input voltage of 5 V_{pp}, the hysteresis response can be observed. When the frequency is swept forwardly, the maximum displacement of approximately 35 nm is found at approximately 131 kHz. However, the maximum displacement magnitude is obtained below 130 kHz, and larger displacement is achieved when the frequency is swept forward than that is swept reverse. With a higher driving voltage of 7 V_{pp}, the PMUT is configured in a highly nonlinear region, and a stronger hysteresis response is obtained. The frequency of maximum displacement magnitude is tuned from 127.5 kHz to 135 kHz, which is a

5.8% shift in frequency domain. Meanwhile, a much larger displacement of about 54 nm is achieved, which is more than 50% larger than the value under 5 V_{pp} driving voltage. To measure the harmonic in terms of the applied voltage, single tone AC frequency of 127.5 kHz was given to the PMUT. The harmonic generations of PMUT under 3 V_{pp} to 7 V_{pp} are shown in right panel of Fig. 8 (a). As the applied voltage is increased, the number of harmonics increases as well. Hence, the study shows that the generations of harmonic can be fully controlled by the applied voltage.

The left panel of Fig. 8 (b) shows the strategy of tuning the frequency to achieve electrically control of the harmonic generations under 9 V_{pp}. Firstly, the hysteresis behavior of displacement is plotted, which exhibits the piezoelectric nonlinearity in AlN-based PMUT. For the forward frequency sweep, a maximum displacement of about 70 nm is achieved, and large frequency shift is also observed from the picture. Since the harmonic generations are dependent on the vibration amplitude, the harmonics are measured under three different frequencies, 100 kHz, 127.5 kHz, and 150 kHz. When the frequency is set to 127.5 kHz, many harmonics can be seen in range of 0-25 MHz. However, few harmonics are obtained under 100 kHz and 150 kHz. According to this observation, the feature can be exploited to achieve tailored number of harmonics.

VII. CONCLUSION

In this paper, the AlN-based PMUT utilizing a five-mask process is fabricated, and the behavior of piezoelectric nonlinearity of AlN thin film in as-fabricated PMUT is successfully characterized. The impedance characteristics are measured, and the electromechanical coupling coefficient k_t^2 is 3.75%. Then, the second order piezoelectric constitutive equations are provided, and the nonlinear piezoelectric coefficient is calculated. Finally, three promising applications, acoustic-optical modulator, frequency comb generator, and electrically controlled harmonic generation, are demonstrated. According to our theoretical and experimental analysis of piezoelectric nonlinearity of AlN thin film, the compacted and low-cost AlN-based PMUT has wide potential applications in acoustic-optical hybrid microsystem and RF communications when driving the AlN thin films into nonlinear region.

REFERENCES

[1] N. B. Gharb and S. Trolier-McKinstry, "Dielectric nonlinearity of $Pb(Yb_{1/2}Nb_{1/2})O_3$–$PbTiO_3$ thin films with 100 and 111 crystallographic orientation," *J. Appl. Phys.*, vol. 97, no. 6, Mar. 2005, Art. no. 064106.

[2] I. Fujii, M. Ugorek, and S. Trolier-McKinstry, "Grain size effect on the dielectric nonlinearity of $BaTiO_3$ ceramics," *J. Appl. Phys.*, vol. 107, no. 10, May 2010, Art. no. 104116.

[3] G.-L. Luo, Y. Kusano, and D. A. Horsley, "Airborne piezoelectric micromachined ultrasonic transducers for long-range detection," *J. Microelectromech. Syst.*, vol. 30, no. 1, pp. 81–89, Feb. 2021.

[4] C. L. E. Bruno, A. S. Gliozzi, M. Scalerandi, and P. Antonaci, "Analysis of elastic nonlinearity using the scaling subtraction method," *Phys. Rev. B, Condens. Matter*, vol. 79, no. 6, Feb. 2009, Art. no. 064108.

[5] N. Aurelle, D. Guyomar, C. Richard, P. Gonnard, and L. Eyraud, "Nonlinear behavior of an ultrasonic transducer," *Ultrasonics*, vol. 34, nos. 2–5, pp. 187–191, Jun. 1996.

[6] G. Robert, D. Damjanovic, N. Setter, and A. V. Turik, "Preisach modeling of piezoelectric nonlinearity in ferroelectric ceramics," *J. Appl. Phys.*, vol. 89, no. 9, pp. 5067–5074, May 2001.

[7] D. Damjanovic and M. Demartin, "The Rayleigh law in piezoelectric ceramics," *J. Phys. D, Appl. Phys.*, vol. 29, no. 7, pp. 2057–2060, Jul. 1996.

[8] H. Yamaguchi, "GaAs-based micro/nanomechanical resonators," *Semicond. Sci. Technol.*, vol. 32, no. 10, Sep. 2017, Art. no. 103003.

[9] G. Pillai and S.-S. Li, "Controllable multichannel acousto-optic modulator and frequency synthesizer enabled by nonlinear MEMS resonator," *Sci. Rep.*, vol. 11, no. 1, p. 13, Dec. 2021.

[10] I. Mahboob, K. Nishiguchi, H. Okamoto, and H. Yamaguchi, "Phonon-cavity electromechanics," *Nature Phys. Lett.*, vol. 8, no. 5, pp. 387–392, Apr. 2012.

[11] J. L. Krause, K. J. Schafer, and K. C. Kulander, "High-order harmonic generation from atoms and ions in the high intensity regime," *Phys. Rev. Lett.*, vol. 68, no. 24, pp. 3535–3538, Jun. 1992.

[12] B. K. McFarland, J. P. Farrell, P. H. Bucksbaum, and M. Gühr, "High harmonic generation from multiple orbitals in N_2," *Science*, vol. 322, no. 5905, pp. 1232–1235, 2008.

[13] Q.-F. Yang, M.-G. Suh, K. Y. Yang, X. Yi, and K. J. Vahala, "Microresonator soliton dual-comb spectroscopy," in *Proc. Conf. Lasers Electro-Opt.*, May 2017, pp. 1–7.

[14] A. Martin, O. Alibart, M. P. De Micheli, D. B. Ostrowsky, and S. Tanzilli, "A quantum relay chip based on telecommunication integrated optics technology," *New J. Phys.*, vol. 14, no. 2, Feb. 2012, Art. no. 025002.

[15] K.-H. Luo *et al.*, "Nonlinear integrated quantum electro-optic circuits," *Sci. Adv.*, vol. 5, no. 1, Jan. 2019, Art. no. eaat1451.

[16] J. Wang, Z. Ren, and C. T.-C. Nguyen, "1.156-GHz self-aligned vibrating micromechanical disk resonator," *IEEE Trans. Ultrason., Ferroelectr., Freq. Control*, vol. 51, no. 12, pp. 1607–1628, Dec. 2004.

[17] S. Pourkamali, A. Hashimura, R. Abdolvand, G. K. Ho, A. Erbil, and F. Ayazi, "High-Q single crystal silicon HARPSS capacitive beam resonators with self-aligned sub-100-nm transduction gaps," *J. Microelectromech. Syst.*, vol. 12, no. 4, pp. 487–496, Aug. 2003.

[18] L.-W. Hung and C. T.-C. Nguyen, "Capacitive-piezoelectric AlN resonators with Q>12,000," in *Proc. IEEE 24th Int. Conf. Micro Electro Mech. Syst.*, Jan. 2011, pp. 173–176.

[19] G. Piazza, P. J. Stephanou, and A. P. Pisano, "Piezoelectric aluminum nitride vibrating contour-mode MEMS resonators," *J. Microelectromech. Syst.*, vol. 15, no. 6, pp. 1406–1418, Dec. 2006.

[20] R. Ruby, "Review and comparison of bulk acoustic wave FBAR, SMR technology," in *Proc. IEEE Ultrason. Symp.*, New York, NY, USA, Oct. 2007, pp. 1029–1040.

[21] T. Wu *et al.*, "Design and fabrication of AlN RF MEMS switch for near-zero power RF wake-up receivers," in *Proc. IEEE Sensors*, Glasgow, Scotland, Oct. 2017, pp. 1–3.

[22] M.-A. Dubois and P. Muralt, "Properties of aluminum nitride thin films for piezoelectric transducers and microwave filter applications," *Appl. Phys. Lett.*, vol. 74, no. 20, pp. 3032–3034, May 1999.

[23] M.-A. Dubois and P. Muralt, "Stress and piezoelectric properties of aluminum nitride thin films deposited onto metal electrodes by pulsed direct current reactive sputtering," *J. Appl. Phys.*, vol. 89, no. 11, pp. 6389–6395, Jun. 2001.

[24] J. Cai, K. Liu, L. Lou, S. Zhang, Y. A. Gu, and T. Wu, "Increasing ranging accuracy of aluminum nitride PMUTs by circuit coupling," in *Proc. IEEE 34th Int. Conf. Micro Electro Mech. Syst. (MEMS)*, Jan. 2021, pp. 740–743.

[25] J. Cai *et al.*, "Photoacoustic and ultrosound dual-modality endoscopic imaging based on ALN PMUT array," in *Proc. IEEE 35th Int. Conf. Micro Electro Mech. Syst. Conf. (MEMS)*, Jan. 2022, pp. 412–415.

[26] S. Wu, W. Li, D. Jiao, H. Yang, T. Wu, and X. Li, "An aluminum-nitride PMUT with pre-concaved membrane for large deformation and high quality-factor performance," in *Proc. 21st Int. Conf. Solid-State Sensors, Actuat. Microsyst., Transducers*, Jun. 2021, pp. 46–49.

[27] M.-H. Li, C.-Y. Chen, R. Lu, Y. Yang, T. Wu, and S. Gong, "Power-efficient ovenized lithium niobate SH0 resonator arrays with passive temperature compensation," in *Proc. IEEE 32nd Int. Conf. Micro Electro Mech. Syst. (MEMS)*, Seoul, South Korea, Jan. 2019, pp. 911–914.

[28] L. Colombo, A. Kochhar, G. Vidal-Álvarez, and G. Piazza, "X-cut lithium niobate laterally vibrating MEMS resonator with figure of merit of 1560," *J. Microelectromech. Syst.*, vol. 27 no. 4, pp. 602–604, Aug. 2018.

[29] K. Prume, P. Muralt, F. Calame, T. Schmitz-Kempen, and S. Tiedke, "Extensive electromechanical characterization of PZT thin films for MEMS applications by electrical and mechanical excitation signals," *J. Electroceram.*, vol. 19, no. 4, pp. 407–411, Dec. 2007.

[30] Z. Luo, S. Shao, and T. Wu, "Characterization of AlN and AlScN film ICP etching for micro/nano fabrication," *Microelectron. Eng.*, vols. 242–243, Apr. 2021, Art. no. 111530.
[31] J. G. Rodríguez-Madrid, G. F. Iriarte, J. Pedrós, O. A. Williams, D. Brink, and F. Calle, "Super-high-frequency SAW resonators on AlN/diamond," *IEEE Electron Device Lett.*, vol. 33, no. 4, pp. 495–497, Apr. 2012.
[32] R. Ruby, P. Bradley, J. D. Larson, and Y. Oshmyansky, "PCS 1900 MHz duplexer using thin film bulk acoustic resonators (FBARs)," *Electron. Lett.*, vol. 35, no. 10, p. 794, 1999.
[33] D. B. Sohn, S. Kim, and G. Bahl, "Time-reversal symmetry breaking with acoustic pumping of nanophotonic circuits," *Nature Photon.*, vol. 12, no. 2, pp. 91–97, Feb. 2018.
[34] S. Ghosh and G. Piazza, "Laterally vibrating resonator based elasto-optic modulation in aluminum nitride," *APL Photon.*, vol. 1, no. 3, Jun. 2016, Art. no. 036101.
[35] E. A. Kittlaus, W. M. Jones, P. T. Rakich, N. T. Otterstrom, R. E. Müller, and M. Rais-Zadeh, "Electrically driven acousto-optics and broadband non-reciprocity in silicon photonics," *Nature Photon.*, vol. 15, no. 1, pp. 43–52, Jan. 2021.
[36] Z. Yu and X. Sun, "Gigahertz acousto-optic modulation and frequency shifting on etchless lithium niobate integrated platform," *ACS Photon.*, vol. 8, no. 3, pp. 798–803, Mar. 2021.
[37] H. Tian *et al.*, "Hybrid integrated photonics using bulk acoustic resonators," *Nature Commun.*, vol. 11, no. 1, p. 3073, Dec. 2020.
[38] H. Li, S. A. Tadesse, Q. Liu, and M. Li, "Nanophotonic cavity optomechanics with propagating acoustic waves at frequencies up to 12 GHz," *Optica*, vol. 2, no. 9, p. 826, Sep. 2015.
[39] S. A. Tadesse and M. Li, "Sub-optical wavelength acoustic wave modulation of integrated photonic resonators at microwave frequencies," *Nature Commun.*, vol. 5, no. 1, p. 5402, Dec. 2014.
[40] H. Tian *et al.*, "Magnetic-free silicon nitride integrated optical isolator," *Nature Photon.*, vol. 15, no. 11, pp. 828–836, Nov. 2021.
[41] S. Shelton, O. Rozen, A. Guedes, R. Przybyla, B. Boser, and D. A. Horsley, "Improved acoustic coupling of air-coupled micromachined ultrasonic transducers," in *Proc. IEEE 27th Int. Conf. Micro Electro Mech. Syst. (MEMS)*, Jan. 2014, pp. 753–756.
[42] E. Ventsel and T. Krauthammer, *Thin Plates and Shells: Theory, Analysis, and Applications*. New York, NY, USA: Marcel Dekker, 2001.

ZHIFANG LUO (Student Member, IEEE) received the B.S. degree in physics from ShanghaiTech University, Shanghai, China, in 2019, where he is currently pursuing the Ph.D. degree in electrical engineering.

His research interests include the design and microfabrication techniques of piezoelectric microelectromechanical system (MEMS) resonators for RF and sensing applications and hybrid microsystems based on the integration of MEMS device with photonics for signal processing.

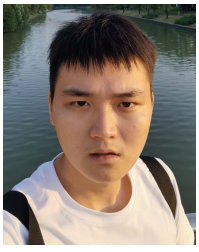

JUNXIANG CAI (Student Member, IEEE) is currently pursuing the Ph.D. degree in electrical engineering with ShanghaiTech University, Shanghai, China. His research interests are the design and manufacture of RF filters and micro/nano sensors based on piezoelectric materials, such as aluminum nitride (AlN) and scandium doped aluminum nitride (AlScN) thin films.

SONGSONG ZHANG received the Ph.D. degree from the Department of Electrical Engineering, National University of Singapore (NUS), in 2014. He was a Research Scientist at the Institute of Microelectronics (IME), A*STAR, from 2014 to 2019. He has joined the Shanghai Industrial μTechnology Research Institute (SITRI) in October 2019 and is currently the Director of the Advanced Acoustic Group (AAG). He is working on the technology development and productization of thin film aluminum nitride (AlN)-based piezoelectric MEMS platform.

YUANDONG (ALEX) GU received the M.E.E. degree in electrical engineering and the Ph.D. degree in pharmaceutics from the University of Minnesota, Minneapolis, MN, USA, in 2001 and 2003, respectively. He is currently the Founding Dean of the School of Microelectronics, Shanghai University, with concurrent appointment as the CTO of the Shanghai Industrial μTechnology Research Institute (SITRI). Before SITRI, he was the Deputy Executive Director of the Institute of Microelectronics (IME), Singapore. Prior to IME, he has spent 11 years at the Honeywell Advanced Technology Labs. His research interests lie in piezoelectric MEMS sensors and MEMS/ASIC monolithic integration.

LIANG LOU received the Ph.D. degree from the Department of Electrical Engineering, National University of Singapore, in 2012. He has worked as a Scientist at the Institute of Microelectronics, A*STAR, from 2012 to 2018. He has been the Director of the Advanced Acoustic Group, Shanghai Industrial μTechnology Research Institute, since September 2018. His research interests include piezoelectric devices and their system integration.

TAO WU (Senior Member, IEEE) received the B.S. degree (Hons.) in electrical engineering from Zhejiang University, China, in 2007, and the M.S. and Ph.D. degrees from the University of California at Los Angeles, Los Angeles, CA, USA, in 2009 and 2011, respectively.

He was a Process TD Engineer with Intel Corporation, Hillsboro, OR, USA, from 2014 to 2015. Then, he was a Post-Doctoral Research Fellow with Stanford University and Northeastern University from 2014 to 2017. He is currently an Assistant Professor at the School of Information Science and Technology, ShanghaiTech University, Shanghai, China. He has authored or a coauthor of more than 60 papers in prestigious IEEE journals and conferences. His research interests include design and fabrication of multiferroic transducers, piezoelectric resonators, and integrated circuit for MEMS-based microsystems.